Viking Pitch Damping Derivatives as Influenced by Support Interference and Test Techniques

SY STEINBERG*
Martin Marietta Aerospace; Denver, Colo.

AND

BOB L. USELTON†
ARO Inc., Arnold Air Force Station, Tullahoma, Tenn.

AND

PAUL M. SIEMERS III‡
NASA Langley Research Center, Hampton, Va.

Sting support interference effects on the pitch damping derivatives and a comparison of damping characteristics using forced and free oscillation test methods were investigated on 140° spherically blunted cone configurations at $M = 1.76$–3.0. Sting influences are minimal with sting/model diameter ratios $= 0.183$ and effective sting lengths $= 3.55\ d_m$. Increasing d_s/d_m to 0.53 provides a considerable influence to the damping parameter at $\alpha = 0°$–$3°$ at all Reynolds numbers but shows little or no effect at higher alphas. A good correlation of free-flight and small diameter sting captive model wake geometries (wake neck position and size) was obtained which adds confidence in obtaining damping derivatives through captive model testing. The damping characteristics obtained on 11.23% and 4.35% scale Viking configurations using forced and free oscillation test methods respectively in two different test facilities are compared. The agreement is quite good at almost all test conditions.

Nomenclature

A = reference area, $\pi d^2/4$, ft^2
C_m = pitching-moment coefficient, $(PM/q_\infty A d_m)$
C_{mq} = $\partial C_m/\partial(qd/2V_\infty)$ pitch damping derivative, 1/rad
$C_{m\dot{\alpha}}$ = $\partial C_m/\partial(\dot{\alpha}d/2V_\infty)$ pitch damping derivative, 1/rad
d_m = reference length (maximum model diameter), ft or in.
d_F, d_s, d_w = sting flare, sting, and wake neck diameter, respectively, in.
l_s = effective sting length, in.
l_w = horizontal distance from maximum model diameter to wake neck, in.
M_∞ = freestream Mach number
PM = pitching moment, in. -lb.
q = pitching velocity, rad/sec
q_∞ = freestream dynamic pressure $(\rho V_\infty{}^2/2)$, psia
Re_{dm} = freestream Reynolds number based on d_m
V_∞ = freestream velocity, fps
x_{cg} = horizontal distance from model theoretical nose to c.g. (pivot axis), in.
z_{cg} = vertical distance from model centerline to c.g. (pivot axis), in.
α = angle of attack, deg
$\dot{\alpha}$ = time rate of change of α, rad/sec
θ = oscillation amplitude, deg
θ_c = model cone half-angle, deg
ρ = mass density of air, slugs/ft^3
ϕ = roll angle, deg
ω = angular frequency, rad/sec
$\omega d_m/2V_\infty$ = reduced frequency parameter, rad

Presented as Paper 72-1012 at the AIAA 7th Aerodynamic Testing Conference, Palo Alto, Calif., September 13–15 1972; submitted September 29, 1972; revision received February 15, 1973. This work was supported by NASA/Langley Research Center Contracts NASI-9000 with Martin Marietta Aerospace, Denver Division, and F40600-72-C-0003 with ARO Inc., Tullahoma, Tenn.

Index categories: Spacecraft Ground Testing and Simulation (including Components); Subsonic and Transonic Flow; Jets, Wakes, and Viscid-Inviscid Flow Interactions.

*Senior Group Engineer, Systems Analysis Department, Martin Marietta Aerospace, Denver Division. Associate Fellow AIAA.

†Project Engineer, Dynamics Group, Aerodynamics Division, von Kármán Gas Dynamics Facility. Member AIAA.

‡Aerospace Technologist, Viking Project Office.

Introduction

THE planned use of several different test techniques to determine the Viking configuration pitch damping was prompted by the unusually large data uncertainties experienced by experimentors[1–4] when the damping of blunted large-angle cone configurations was sought. The differing techniques included captive model resonant frequency single degree-of-freedom forced and free oscillation systems,[5] and ballistics range[1,6] or free flight in wind tunnel[4,7] test methods. The latter technique involves the study of the scaled model time-dependent motion through continuous motion picture coverage (recently developed for two-plane coverage permitting determination of model coning motion, if present). Each test technique has advantages and disadvantages. The experimentor must critically evaluate all known techniques and base his selection on compatibility with test objectives. Regardless of test method used for such configurations, an accurate measurement is difficult to obtain, particularly at lower alphas, as evidenced by the relatively large data uncertainty obtained during test.

The work of Reding and Ericsson[8] suggested several elements that may influence the dynamic damping derivative. This paper examines support interference as a prime candidate for distorting pitch damping. In addition, damping data involving different test methods (both forced and free oscillation) are examined and compared. The latter study involves geometrically-similar models of two different scales tested in two different wind tunnel facilities in identical test environments. This paper also presents some data containing inconsistencies and offers judgments as to the cause of these anomalies.

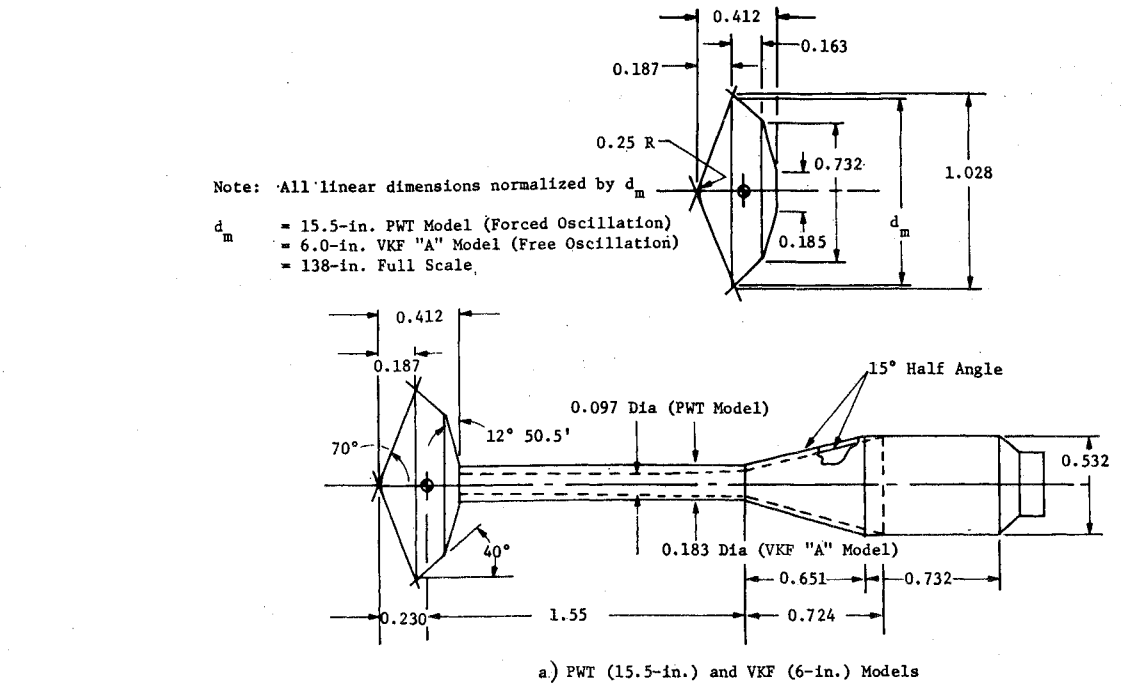

a) PWT (15.5-in.) and VKF (6-in.) Models

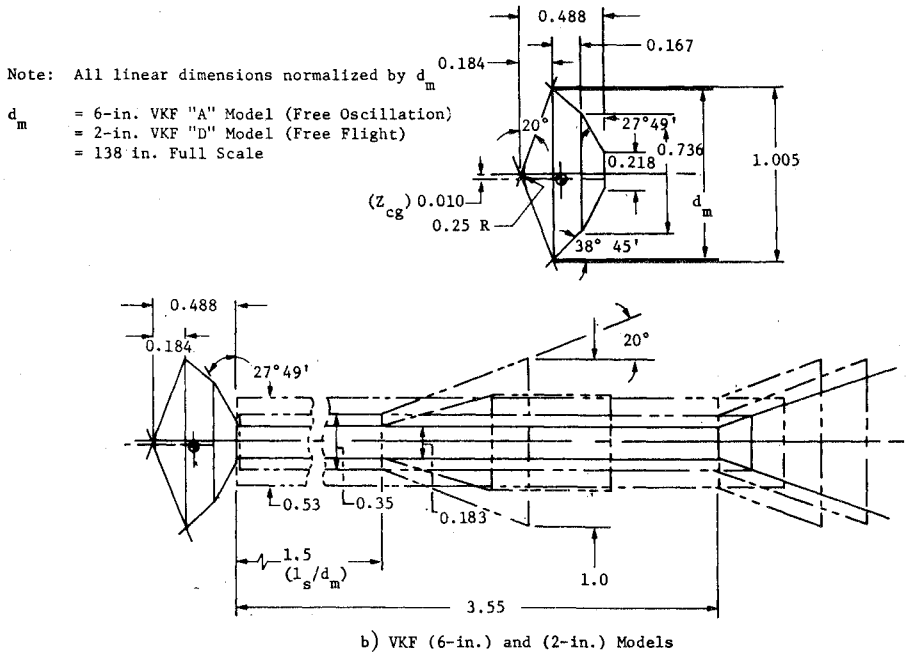

b) VKF (6-in.) and (2-in.) Models

Fig. 1 Model and support sting geometry.

Pitch damping tests[9,10] were conducted in 1971 at the Arnold Engineering Development Center von Kármán Gas Dynamics Facility (VKF) Tunnel A on 4.35% scale models of both early (Fig. 1a) and current (Fig. 1b) Viking configurations. These tests, conducted at $M = 1.75$–3.0, used the sting supported free oscillation test technique and included sting geometry variation permitting an evaluation of support interference effects. Although these data pertain to 140° spherically blunted cone configurations, they are judged equally applicable to all large angle cone forebody configurations having typical afterbodies. In addition to these captive model tests, 1.45% scale model (Fig. 1b) free-flight tests were conducted at VKF Tunnel D at $M = 1.6$–3.0. This provided wake geometries which permits comparison with those from captive model tests and thus the wake distortion (in a qualified sense) caused by the sting. The Tunnel A damping data are compared with prior data[11,12] obtained in the AEDC PWT 16 ft tunnels. These earlier Viking configuration (Fig. 1a) forced oscillation tests involved 11.23% scale models and provided the basis for comparing data obtained by two test methods using two different subscale captive models in different facilities.

Test Techniques and Models

Forced Oscillation System

The transonic and supersonic dynamic damping tests conducted in the PWT facilities involved using the forced oscillation test technique. The forced oscillation balance[5] is a small-amplitude, one degree-of-freedom, resonant frequency,§ oscillatory system incorporating a cross-flexure pivot. The sting-supported balance is oscillated by an electromagnetic

§It can also be operated off-resonance.

shaker motor providing constant model oscillation amplitudes of $\pm 1.8°$. Strain gage bridges measure the model angular displacements and the system input torque. These data are recorded on magnetic tape for subsequent data reduction. The forcing system is equipped with a feedback control network to provide positive amplitude control for testing either dynamically stable or unstable configurations.

Free Oscillation System

The supersonic tests conducted in the VKF Tunnel A facility used a small-amplitude, one degree-of-freedom, free oscillation sting-supported balance system[5] incorporating a cross-flexure pivot. An air jet is used for initial displacement of stable configurations. The air jet is emitted from a tube by a remote controlled servo valve oscillating at the natural frequency of the model balance system. At the desired oscillation amplitude, the driving force is abruptly stopped by a solenoid valve and the digitized displacement signal is recorded on magnetic tape for later data reduction. If the model is dynamically unstable, it is unlocked and data are recorded on tape as the model oscillation amplitude diverges. The oscillation amplitude range used is approximately $\pm 2.4°$ to $\pm 0.6°$; the log decrement method was used for data reduction.

Free Flight

The free-flight models are supported on the tunnel centerline by a horizontal wire which runs through the model base cover. After tunnel flow is established, the wire is broken at a notch inside the model. The wires are quickly and automatically withdrawn, leaving the model in free flight within the test section. Its motion is photographed with the tunnel schlieren system at approximately 5000 frames/sec. The film provides model wake geometry and model acceleration from which drag is calculated.

Models

The geometry of both the early and current Viking configurations and their respective sting support arrangements are shown in Fig. 1a and b. The current Viking configuration geometry (Fig. 1b) also applies to the free-flight-model. The PWT test model (15.5 in. diam) was constructed of aluminum; the VKF scaled model of the PWT configuration (6 in. diam) was made of stainless steel. The sting arrangements are contrasted in Fig. 1a. The current Viking configuration (6 in. diam) was constructed of Mallory®, a sintered tungsten alloy of high density, (0.614 lb/in.^{3}) to provide a high moment of inertia. The free-flight models (2 in. diam) were made of aluminum.

The sting interference study was conducted on the 6-in.-diam current Viking configuration model. The baseline sting-model diameter ratio is 0.183. Aluminum sleeves are provided to fit over the basic sting to also give d_s/d_m values of 0.35 and 0.53. The sting flare was also adjustable to provide effective sting length ratios (l_s/d_m) of 1.50 and 3.55.

Discussion of Results

Support Interference Evaluation

Wake geometry comparison

Schlieren photographic coverage was used during free-flight tests (2-in. models) in VKF "D" and the free oscillation investigations (6-in. model) in VKF "A." Summary plots of wake geometry are presented in Fig. 2 in terms of both minimum wake diameter (d_w/d_m) and wake length (l_w/d_m) as a function of Mach number. Both free flight and captive model data are presented and may be directly compared in spite of Reynolds number variation with Mach number. No significant effect of Reynolds number on wake geometry was found for any free-flight or sting-supported model tests except for the short length sting configuration.

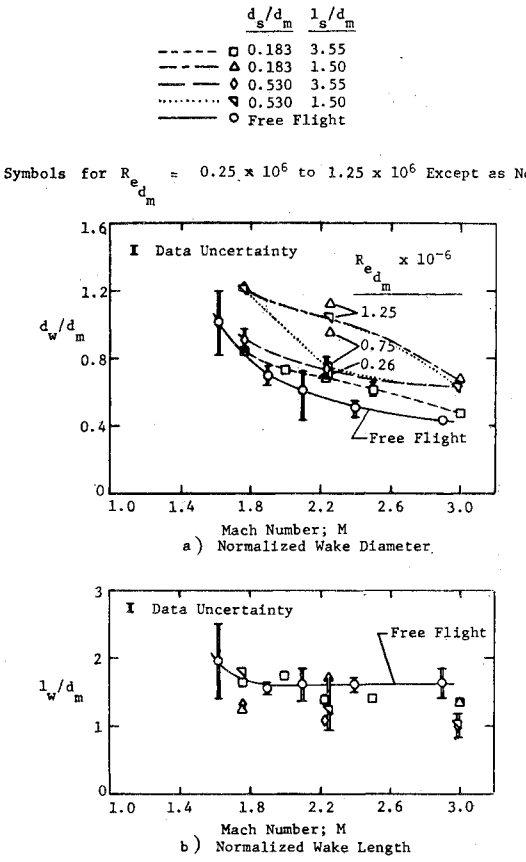

Fig. 2 Wake geometry as a function of Mach number.

The sting is responsible for forcing the wake diameter outward. Sting configuration and Mach number have a large influence on wake diameter as exemplified in Fig. 2a. In general, minimum sting diameter and maximum effective sting length (square symbols) provide for the least influence, as was anticipated. At $M \approx 1.7$ sting diameter has only a minimum influence on wake geometry in contrast to sting effective length which is seen to have a large effect. At $M \approx 3.0$ sting length had virtually no effect on the data for the large sting but shows a considerable influence with the small sting. Also noted in this figure is the large Reynolds number effect on wake diameter at $M \approx 2.2$. Judgments relating to this and other data anomalies at this Mach number will be discussed later.

The free-flight wake length (Fig. 2b) is basically constant above $M \approx 1.9$; in the lower Mach number range, the blown wake makes the length poorly defined. The shorter wake lengths obtained with the sting-mounted model occur because less length is required for wake contraction to the larger wake diameters, assuming identical contraction angles. In comparing lengths obtained from free flight and sting-mounted model tests, it is seen that the wake geometry was not appreciably altered by use of the baseline sting ($d_s/d_m = 0.183$, $l_s/d_m = 3.55$).

Sting Effects on Damping Parameter

The largest sting support influences on the dynamic damping parameter, are found to occur at the lowest test Mach number (1.76) for which this interference study was made. The data presented will therefore be restricted to $M = 1.76$ but the reader should understand that the effects noted at 1.76 are typically larger than at higher Mach numbers. In

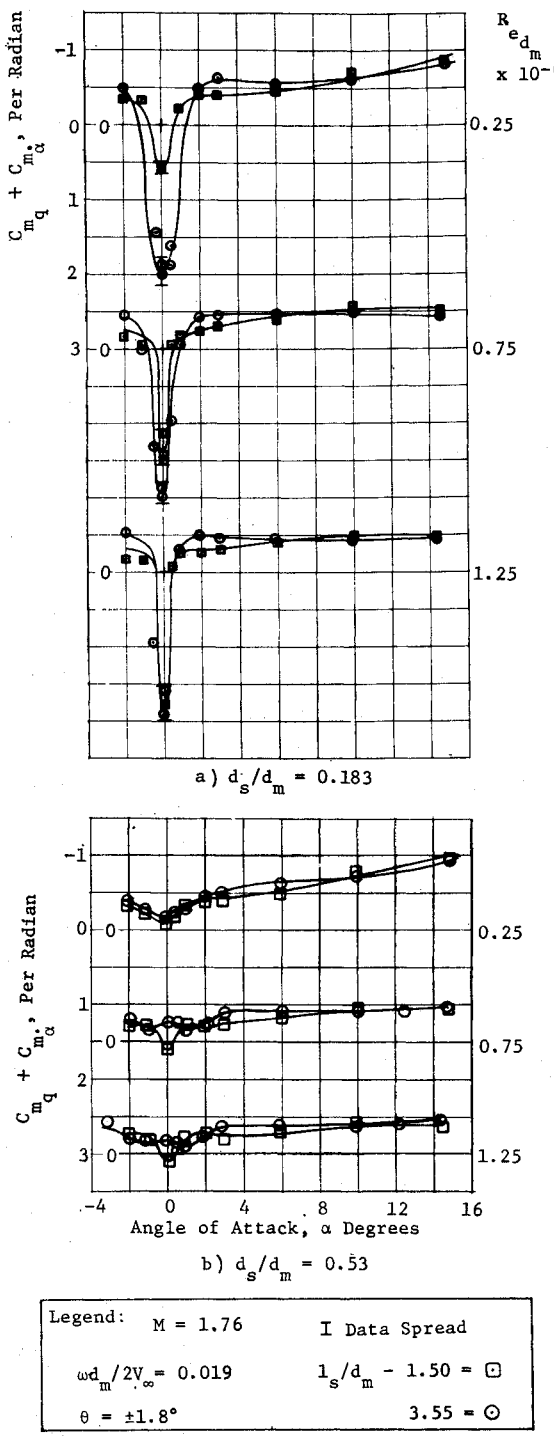

Fig. 3 Dynamic damping parameter comparison at two sting length ratios as a function of angle of attack.

fact, the data obtained at $M = 2.23$ show small effects of effective sting length and diameter while the data at $M = 3.0$ showed no interference effects for the tested conditions.

Figure 3 presents a comparison of the damping parameter $(C_{m_q} + C_{m_{\dot{\alpha}}})$ as a function of alpha for two effective sting length ratios at two sting diameters over the test Reynolds number range. Sting length effects appear minimal within the data accuracy band for all test conditions and both sting diameters above $\alpha = 3°$. In fact, the largest sting diameter appears to provide results which are insensitive to sting length at all angles of attack. The greatest influence of sting length is evident at $Re_{d_m} = 0.25 \times 10^6$ below $\alpha = 3°$, and minimally at $Re_{d_m} = 0.75 \times 10^6$ at α near 0°, for $M = 1.76$. The effects are more clearly evident in the cross-plots of Fig. 4, where the damping parameter is plotted as a function of sting-length ratio for several constant angles of attack. The curve slopes $\{\partial(C_{m_q} + C_{m_{\dot{\alpha}}})/\partial(l_s/d_m)\}$ are zero or near zero in all cases except at $Re_{d_m} = 0.25 \times 10^6$ for the small diameter sting. There is an unstable damping trend as effective sting length increases at $\alpha = 0°$ and 1° for this test case. It is evident that a short sting of relatively large diameter with respect to model diameter prevents the natural formation of a blunt body wake (Fig. 2) as contrasted to free-flight model wakes. This relates to a long, small-diameter sting which provides minimal interference to normal body wake formation. Evidently, larger diameter stings create a wake typical of that expected from models of greater fineness ratio which provides for increased damping near $\alpha = 0°$. A normal blunt body wake therefore is the major contributing element to unstable damping, particularly at small angles of attack. Further substantiating evidence, attesting to the wake flow being the source of low alpha unstable damping, lies in the normal

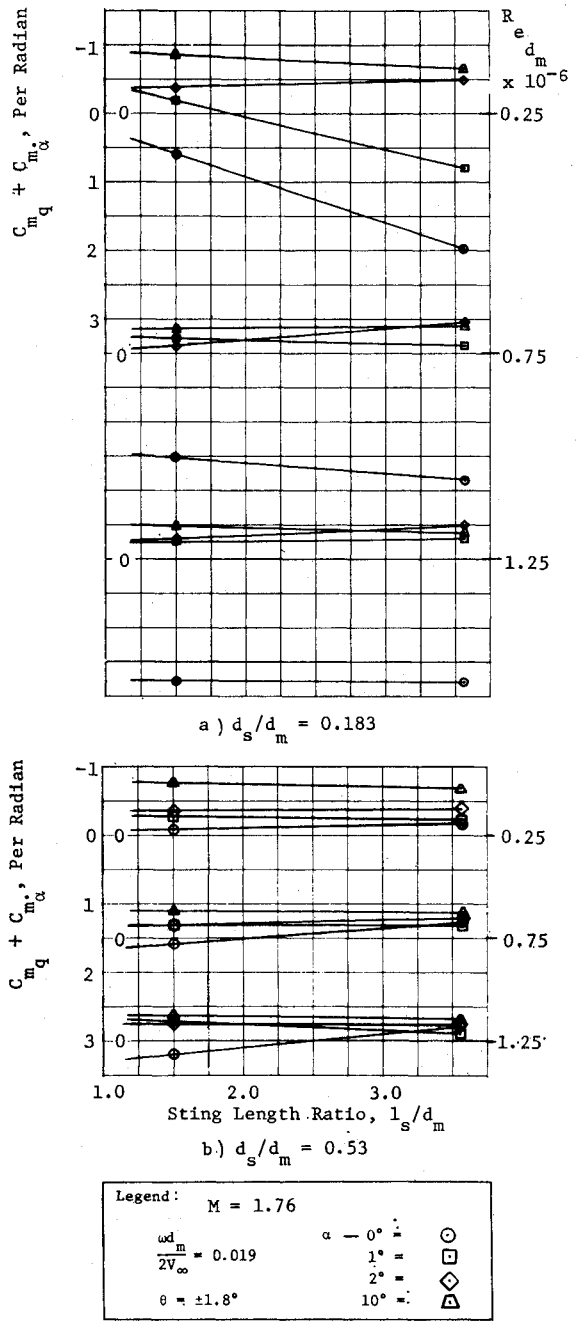

Fig. 4 Dynamic damping parameter as a function of sting length ratio for several angles of attack.

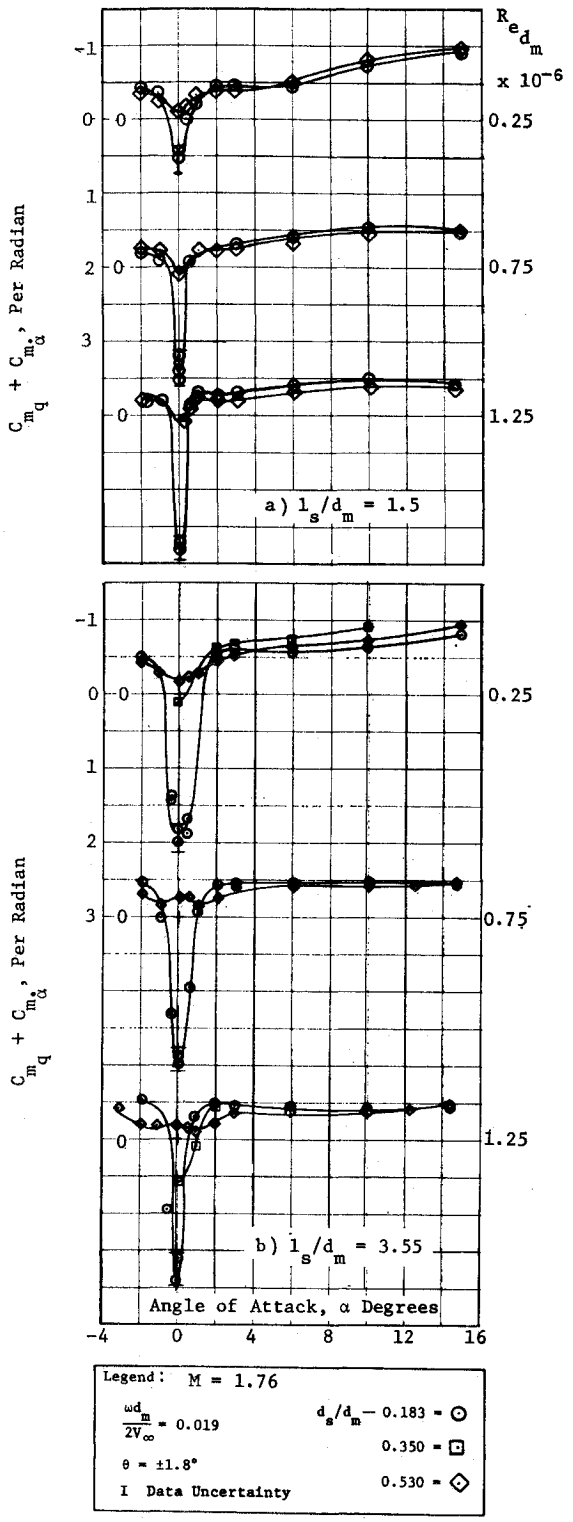

Fig. 5 Dynamic damping parameter comparison for normalized sting diameter as a function of angle of attack.

force curve for these blunted conical configurations. At small angles of attack and over the Mach range from about $M = 0.7$ to approximately 2.3,[13-15] the normal force coefficient is either negative or near zero depending on Mach number. This condition exists because of a net down load on the afterbody in the static case. If one can envision an unsteady down load on the afterbody in this nonlinear force region aft of the pivot axis (c.g.), the source of the unstable damping becomes evident. It is judged that a relatively small diameter sting of reasonable length ($d_s/d_m = 0.183$, $l_s/d_m =$ 3.55) should provide for no damping interference for the Viking configuration.

Figures 5 and 6 present the effects of normalized sting diameter upon the dynamic damping parameter at $M = 1.76$. Figure 5 shows the parameter effect as a function of α for several Re_{d_m} and two l_s/d_m values. Figure 6 represents crossplots of Fig. 5 at several angles of attack with the damping parameter presented as a function of normalized sting area. Just as was shown for the sting length influence above $\alpha \approx 2°$, the sting diameter likewise has minimal influences upon the results. Below $\alpha \approx 2°$, however, there is indicated sting interference at all test Reynolds numbers. This is evidenced by

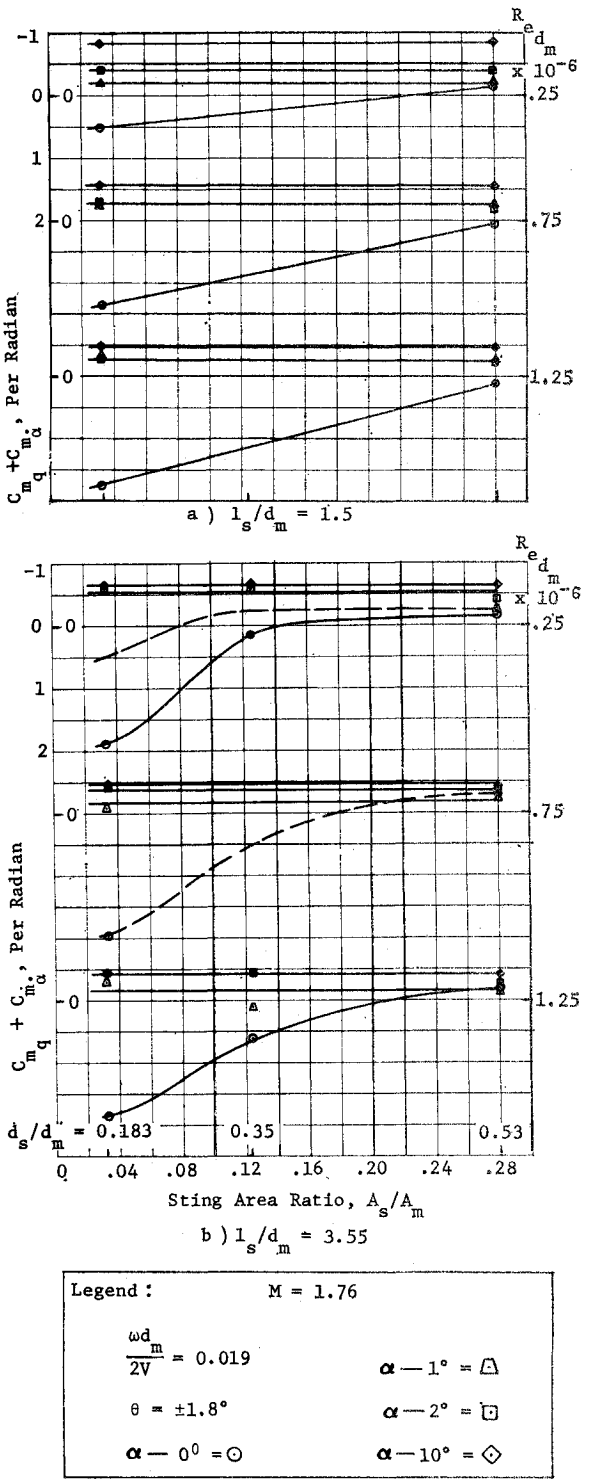

Fig. 6 Dynamic damping parameter as a function of noramalized sting area for several angles of attack.

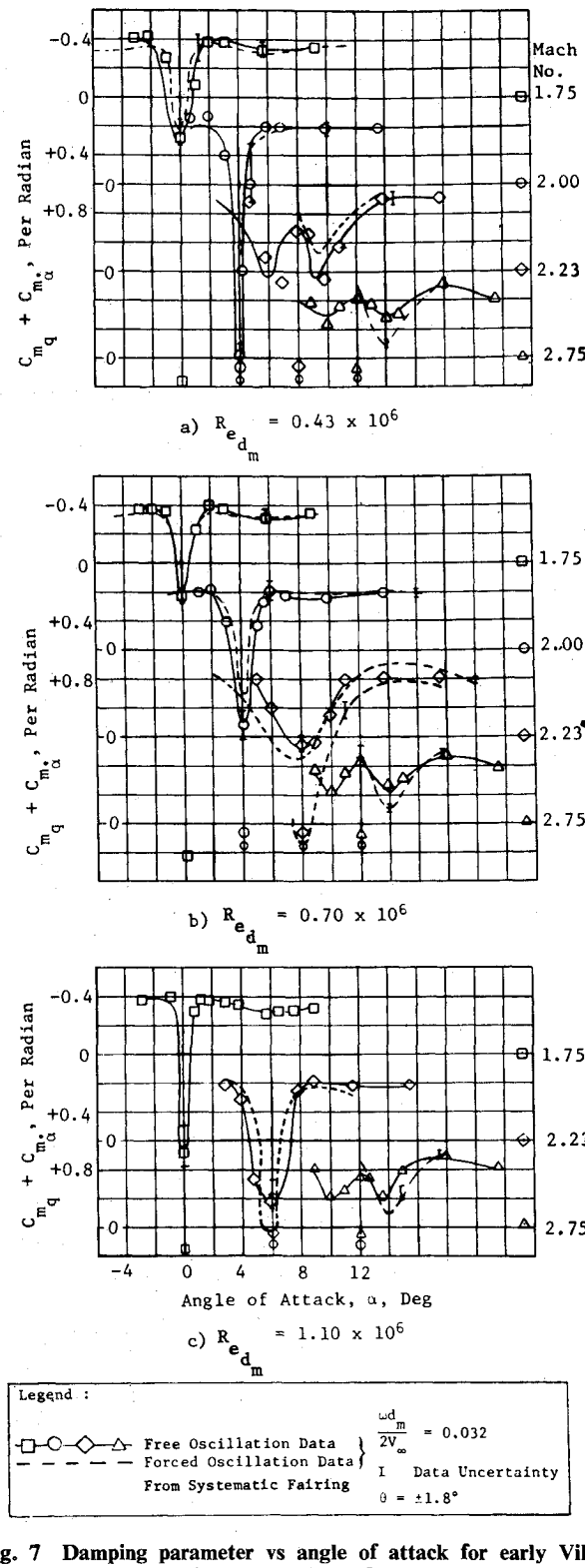

Fig. 7 Damping parameter vs angle of attack for early Viking configuration; comparison of test methods.

the unstable trend as normalized sting area is reduced and is unlike the sting length results which only showed an influence at $Re_{d_m} = 0.25 \times 10^6$. The results show unstable damping spikes with the smallest sting tested. Although there is insufficient data to confidently extrapolate the results to zero sting diameter, it is believed that further reductions in sting diameter would not have altered the damping. This judgment is based on the very good agreement of damping data obtained with the early Viking configuration, comparing the two test methods (Fig. 7), discussed in the next section. In this data comparison it is seen that forced and free oscillation data compared very well, although the test models were of different scale and were tested in different facilities. The two normalized sting diameters did differ, however (Fig. 1a), and the inference is that sting diameter influences are minor or nonexistent at d_s/d_m values below 0.183.

It is judged that these sting support interference data are applicable to large-angle cone forebody configurations with typical afterbody such as Viking. It is conceivable that larger afterbody shapes might be more sensitive to sting interference than smaller protruding afterbodies.

Comparison of Forced and Free Oscillation Data

A philosophical objective of all planned Viking damping tests included obtaining confidence in the data. The data uncertainty bands experienced were shown to be indepedent of test method and were generally typical for these configurations.[1-4,6,9-12] A good data correlation for the same configuration, but obtained by somewhat different methods on different model scales and in different facilities, would add greatly to data confidence. This increased confidence is exemplified in the data of Figs. 7 and 8. The comparison is for

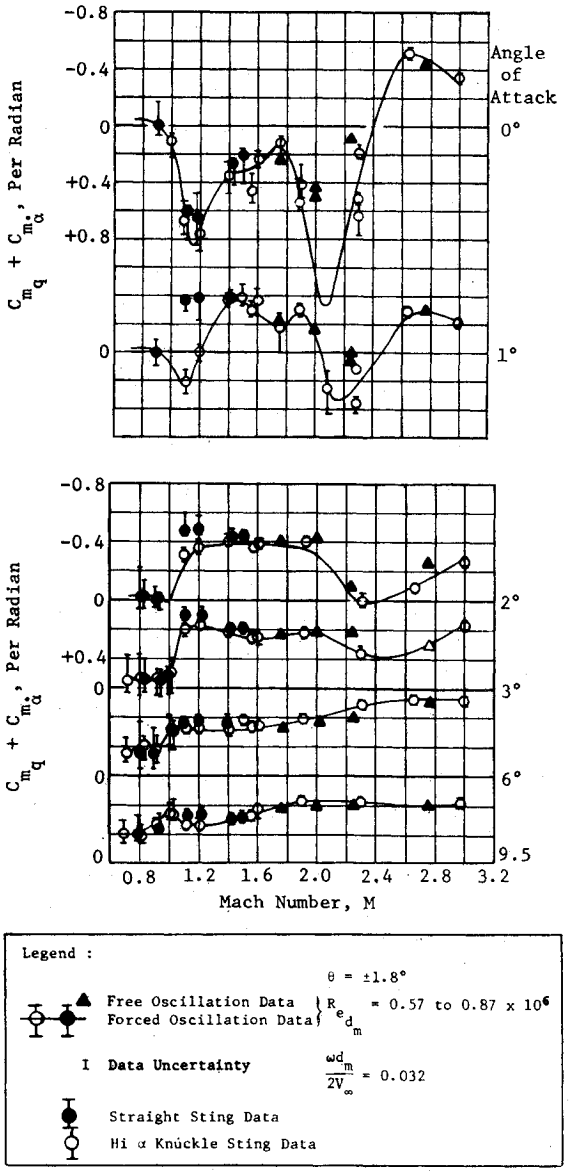

Fig. 8 Damping parameter at constant α vs Mach number for early Viking configuration; comparison of test methods.

forced vs free oscillation test methods and model scales of 11.23% and 4.35%. These models were tested in PWT and VKF tunnels, respectively, at closely matched test conditions. The model(s) sting arrangement is compared in Fig. 1a. The relative sting-model diameter ratios for each model (PWT = 0.097; VKF = 0.183) represent the only difference in geometric arrangement. This difference is considered insignificant on the basis of both the effects of sting diameter already shown and the good correlation of data which will now be discussed.

Figure 7 compares the damping parameter for each test method as a function of angle of attack at constant Mach number for several Reynolds numbers. With the exception of a repeat set of data at $M = 2.23$, $Re_{d_m} = 0.70 \times 10^6$, the agreement of data are quite good. The repeat data will be referred to in a later paragraph. It should be noted that data uncertainties appear greater at $M = 2.23$ than at other Mach numbers as is evident in Fig. 8 which presents the PWT data curves[11,12] in terms of the damping parameter plotted as a function of Mach number at constant α. Superimposed on these plots are the VKF[9,10] data (darkened triangles) so that forced and free oscillation test data may be directly compared. It is apparent that the data comparisons at all angles of attack are quite good and that the $M = 2.23$ data show the largest discrepancy when contrasted to data at other Mach numbers.

The PWT data presented in Fig. 8 warrants additional discussion. The darkened circle points represent data obtained in PWT 16T using a straight sting arrangement in contrast to an adjustable knuckle sting arrangement, which provided data represented by the open circles. The physical difference in sting arrangement lies in an adaptor section aft of the sting flare shown in Fig. 1a; an adjustable knuckle, which permitted manual settings and corresponding extensions to the test angle range, was present in this location for most of the testing in PWT. A straight sting adaptor replaced the adjustable knuckle for a few test runs. The corresponding data comparison at $\alpha = 1°$, 2° and 3° is not good. These discrepancies are, in part, attributable to support system resonance differences with each sting arrangement and the inability to accurately resolve damping in regions of rapid damping change.

Further examination of the Fig. 8 data reveal two distinct groupings of open circle symbol test data (PWT) at $M \approx 2.3$ and $\alpha = 0°$ and 1°. These data were obtained during different test days at identical test conditions. No conclusive explanation for this anomaly is offered but it should be noted that one set of the data does match the VKF data.

Conclusions

Several wind-tunnel investigations involving the Viking configuration pitch damping characteristics were run over a Mach number range of 0.6 to 3.0. The tests were carried out at several facilities at the Arnold Engineering Development Center including PWT 16T and 16S, and VKF tunnels A and D. Two different test methods for obtaining the configuration pitch damping derivatives were used with two different subscale captive models; the single degree-of-freedom resonant frequency test techniques used were forced oscillation (PWT 16T and S) and free oscillation (VKF A). Both used dynamic cross-flexure balances developed at VKF. Another investigation (VKF D) involved the method of free flight to study wake flow geometry. Primary test objectives addressed in this paper include the effects of model support interference on the dynamic damping derivatives and a comparison of configuration dynamic damping using two test methods. The major conclusions based upon these objectives follow. 1) A comparison of wake geometries (wake neck position and size) based on schlieren photos contrasting free-flight and captive model test results reveals small differences when a sting of $d_s/d_m = 0.183$ and $l_s/d_m = 3.55$ is used. 2) Effects of sting length on the current Viking configuration damping derivative are negligible for most conditions tested; only at angles of attack near zero at $M = 1.76$ and $Re_{d_m} \approx 0.25 \times 10^6$ and 0.75×10^6 are sting length influences upon damping significant. 3) Sting diameter has little or no influence on the damping derivative above about $\alpha = 2°$ for effective sting length ratios of 1.5 and 3.55 at all Mach numbers; near $\alpha = 0°$, however, decreasing relative sting diameter ratio provides for increasingly unstable spikes at all test Reynolds numbers at $M = 1.76$. 4) The damping characteristics of geometrically-similar models of different scales obtained in different facilities by different test methods showed good agreement.

References

[1] Krumins, M. V., "Drag and Stability of Various Mars Entry Configurations," *Proceedings of the 19th Congress of the International Astronautical Federation*, Pergamon Press, Elmsford, N.Y., 1970, IAF Paper RE 138.

[2] Whitlock, C. H., Bendura, R. J., and Henning, A. B., "Dynamic Stability Characteristics of Large-Size 120° Blunted Conical Spacecraft in a Simulated Martian Environment," AIAA Paper 69-104, New York, 1969.

[3] Bendura, R. J., "Low Subsonic Static and Dynamic Stability Characteristics of Two Blunt 120° Cone Configurations," TN D 3853, Feb. 1967, NASA.

[4] Marko, W. J., "Transonic Dynamic and Static Stability Characteristics of Three Blunt-Cone Planetary Entry Shapes," TR 32-1357, Sept. 1, 1969, Jet Propulsion Lab., Pasadena, Calif.

[5] Schueler, C. J., Ward, L. K., and Hodapp, A. E., Jr., "Techniques for Measurement of Dynamic Stability Derivatives in Ground Test Facilities," AGARDograph 121, Oct. 1967.

[6] Sammonds, R. I., "Dynamics of High Drag Probe Shapes at Transonic Speeds," TN D-6489, Sept. 1971, NASA.

[7] Prislin, R. H., "Free-Flight and Free-Oscillation Techniques for Wind Tunnel Dynamics Stability Testing," TR 32-878, March 1, 1966, Jet Propulsion Lab., Pasadena, Calif.

[8] Reding, J. P. and Ericsson, L. E., "Dynamic Support Interference—Fact or Fiction?," AIAA Paper 71-277, Albuquerque, N. Mex., 1971.

[9] Uselton, B. L. and Wallace, A. R., "Damping-In-Pitch and Drag Characteristics of the Viking Configuration at Mach Numbers from 1.6 through 3.0," AEDC-TR-72-56, May 1972, Arnold Air Force Station, Tullahoma, Tenn.

[10] Steinberg, S. and Surline, J. T., "Single Degree of Freedom Pitch Damping for the Viking BLDT Configuration at Mach Numbers from 1.75 through 3.0," TR-3720180, Oct. 1971, Martin Marietta Corp., Denver, Colo.

[11] Steinberg, S., "Experimental Pitch Damping Derivatives for Candidate Viking Entry Configurations at Mach Numbers from 0.6 through 3.0," TR 3709005, June 1970, Martin Marietta Corp., Denver, Colo.

[12] Uselton, B. L., Shadow, T. O., and Mansfield, A. C., "Damping-In-Pitch Derivatives of 120- and 140-Degree Blunted Cones at Mach Numbers from 0.6 through 3.0," AEDC-TR-70-49, April 1970, Arnold Air Force Station, Tullahoma, Tenn.

[13] McGhee, R. J., Siemers, P. M., III, and Pelc, R. E., "Transonic Aerodynamics Characteristics of the Viking Entry and Lander Configurations," TMX-2354, Sept. 1971, NASA.

[14] Blake, W. W., "Transonic Aerodynamic Characteristics and Pressure Distributions on 8 Percent Scale Models of the Viking Lander Capsule, Aeroshell and Lander Plus Base Cover, Vol. I, Test Scope, Aerodynamic Characteristics and Wake Data," TR3720074, Feb. 1971, Martin Marietta Corp., Denver, Colo.

[15] Blake, W. W., "Experimental Aerodynamic Characteristics of the Viking Entry Vehicle Over the Mach Range 1.5–10.0," TR 3720106, April 1971, Martin Marietta Corp., Denver, Colo.